

DOI: 10.1002/cssc.201300218

Niko Aarne, Janne Laine, Tuomas Hänninen, Ville Rantanen, Jani Seitsonen, Janne Ruokolainen and Eero Kontturi. 2013. "Controlled hydrophobic functionalization of natural fibers through self-assembly of amphiphilic diblock copolymer micelles." *ChemSusChem* 7 (6): 1203–1208. © 2013 Wiley-VCH Verlag. Reprinted by permission of John Wiley & Sons.

Controlled Hydrophobic Functionalization of Natural Fibers through Self-Assembly of Amphiphilic Diblock Copolymer Micelles

Niko Aarne,^[a] Janne Laine,^[a] Tuomas Hänninen,^[b] Ville Rantanen,^[c] Jani Seitsonen,^[d] Janne Ruokolainen,^[d] and Eero Kontturi*^[a]

The functionalization of natural fibers is an important task that has recently received considerable attention. We investigated the formation of a hydrophobic layer from amphiphilic diblock copolymer micelles [polystyrene-block-poly(N-methyl-4-vinyl pyridinium iodide)] on natural fibers and on a model surface (mica). A series of micelles were prepared. The micelles were characterized by using cryoscopic TEM and light scattering, and their hydrophobization capability was studied through contact angle measurements, water adsorption, and Raman imaging. Mild heat treatment (130 °C) was used to increase the hydrophobization capability of the micelles. The results showed that the micelles could not hydrophobize a model surface, but could render the natural fibers water repellent both with and without heat treatment. This effect was systematically

studied by varying the composition of the constituent blocks. The results showed that the micelle size (and the molecular weight of the constituent diblock copolymers) was the most important parameter, whereas the cationic (hydrophilic) part played only a minor role. We hypothesized that the hydrophobization effect could be attributed to a combination of the micelle size and the shrinkage of the natural fibers upon drying. The shrinking caused the roughness to increase on the fiber surface, which resulted in a rearrangement of the self-assembled layer in the wet state. Consequently, the fibers became hydrophobic through the roughness effects at multiple length scales. Mild heat treatment melted the micelle core and decreased the minimum size necessary for hydrophobization.

Introduction

The use of natural, plant-based fibers for new functional materials has recently gained much attention.^[1–4] For example, inexpensive medical diagnostics on paper substrates is an emerging area,^[4–10] and there are current efforts to utilize paper as a platform for low-cost electronics.^[11–14] In addition, cellulosic fibers are regarded as the optimal raw material for functional wear, which is redefining our idea of clothing.^[15–18] These advanced concepts often require surface hydrophobicity for successful implementation.^[19] Therefore, the inherent hydrophilic and hygroscopic character of naturally occurring

fibers has proven to be an obstacle, which continues to reduce the potential of plant-based fibers in modern materials science. The community requires a platform method to hydrophobize fibers in a controlled way, preferably in aqueous medium. This study aims at filling this gap by introducing a conceptually new approach: molecularly controlled self-assembly of diblock copolymer micelles on fiber surface, starting from hydrophilic fibers and resulting in fibers with tunable hydrophobicity and advancing water contact angles ranging from 120° to 150°.


The use of plant-based fibers dates back several millennia; therefore, several methods exist for their hydrophobization. The paper industry traditionally utilizes polymer-stabilized dispersions with alkenyl succinic anhydride and alkyl ketene dimers for hydrophobization.^[20,21] However, these methods possess some problems, for example extensive fouling,^[22] and they may not be suitable for the novel applications of natural fiber products. Modern technologies use, for example, polymer^[23] or silicone^[24] layers to achieve the necessary water repellence for more advanced applications. For diagnostic purposes, the surface modification methods have ranged from simple inorganic^[25] or plastic^[26] coatings to highly accurate printing methods.^[27,28] Unfortunately, the coating methods have difficulty in obtaining layers with the desired thickness, and the plastic coatings are not compatible with the largely hydrophilic cellulose substrates. In this work, amphiphilic diblock copolymer micelles have been utilized to obtain controlled hydrophobicity on wood-based fibers. Amphiphilic

[a] N. Aarne, Prof. J. Laine, Dr. E. Kontturi
Department of Forest Products Technology
School of Chemical Technology, Aalto University
P.O. Box 16300, 00076 Aalto (Finland)
E-mail: eero.kontturi@aalto.fi

[b] Dr. T. Hänninen
Biomaterial Applications
VTT Technical Research Centre of Finland
P.O. Box 1000, 02044 VTT (Finland)

[c] V. Rantanen
Research Programs Unit, Genome-Scale Biology and
Institute of Biomedicine, Biochemistry and Developmental Biology
University of Helsinki, P.O. Box 7138, 01051 Helsingin Yliopisto (Finland)

[d] Dr. J. Seitsonen, Prof. J. Ruokolainen
Molecular Materials
Department of Applied Physics, School of Science, Aalto University
P.O. Box 15100, 00076 Aalto (Finland)

 Supporting Information for this article is available on the WWW under <http://dx.doi.org/10.1002/cssc.201300218>.

block copolymer micelles are practical for use in aqueous solutions, in which they can be used to store lyophilic substances inside the hydrophobic core.^[29]

Here, the procedure of applying micelles for hydrophobization occurred in a simple one- or two-step procedure without any additives: (i) the diblock copolymer micelles were self-assembled on a fiber surface from aqueous solution, and (ii) the subsequent mixture was heated above the glass transition temperature (T_g) of the micelle core, which caused the micelles to open, exposing the hydrophobic core to the exterior of the fiber. Because the self-assembly process was performed in the wet state, after which the fibers were dried, step (i) could utilize the well-reported morphological changes of fibers upon drying,^[30] with a different end result from the previous attempts to modify cellulosic surfaces with block copolymers.^[31,32] The roughening of the fiber surface upon drying rendered the surface ultrahydrophobic with larger micelle sizes; this could occur even without the micellar opening. Overall, because of the multiple length scales in roughness with native cellulosic fibers, much higher hydrophobicity could be achieved than when using block copolymer micelles on smooth model surfaces, including cellulose.^[32] Because the self-assembly of the micelles on the fibers was governed by electrostatically driven adsorption, the extent of subsequent hydrophobicity could be tailored with high precision. To demonstrate the molecular control over the phenomenon, we also performed the procedure on a model substrate (mica).

Results and Discussion

Extensively studied, commercially available polystyrene-block-poly(N-methyl-4-vinyl pyridinium iodide), denoted PS-*b*-P4VPQ, was chosen as the amphiphilic block copolymer (Figure 1a).^[33–38] Its N-methyl-4-vinyl pyridinium (P4VPQ) block bears a permanent cationic charge that facilitates adsorption on anionic surfaces, such as mica and cellulosic fibers, which were used in this study. To control the eventual hydrophobicity, polystyrene (PS) blocks of five different lengths were used to prepare the micelles (Figure 1b). Based on previous studies, we chose an exponentially increasing length for the PS blocks rather than a linear increase.^[33,39] The exponentially growing number of PS monomers allowed us to evaluate the dependence of the hydrophobic PS block on the eventual hydrophobization. The small chain length for the cationic block was chosen to minimize the hydrophilic content of the polymer and yet to have enough cationic blocks to obtain irreversible electrostatic adsorption on anionic fibers. The length of the hydrophilic block was kept constant, except for one polymer sample (Block-4, Figure 1c), to investigate the effect of the P4VPQ block on self-assembly and hydrophobization. All PS-*b*-P4VPQ polymers were insoluble in water, which enabled the preparation of micelles through a solvent exchange procedure.^[33] We prepared spherical micelles that had the advantage of uniformity (polydispersity index < 1.1). Furthermore, the micelles were isotropic, that is, the adsorption of the micelles on

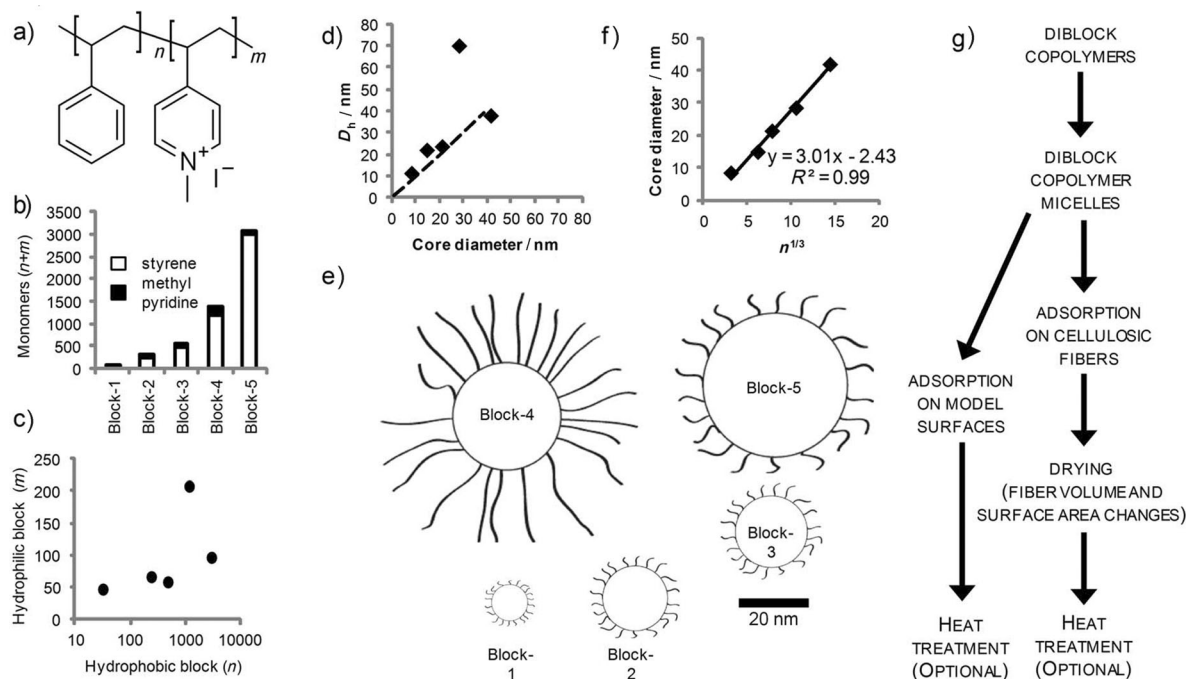


Figure 1. The properties of the block copolymers and the micelles produced from these polymers. a) Chemical structure of the block copolymer: n polystyrene and m PS-*b*-P4VPQ units. b) The five chosen block copolymers showing the total monomer content ($n+m$) divided between styrene and methyl pyridine. c) The hydrophilic block length (m) plotted against the hydrophobic block length (n), which explicitly demonstrates the almost constant hydrophilic block length for the micelles and the exponentially larger hydrophobic blocks. d) The measured hydrodynamic diameter (D_h) and the core diameter exhibit a one-to-one relationship (dashed line) for all but one block copolymer micelle. e) To scale representations of the block copolymer micelles. f) Cubic root of the core block (n), demonstrating a linear relationship with the measured core diameter. g) Experimental outline.

a substrate did not depend on the orientation of the micelles, simplifying the interpretation of the results.

The micelles were characterized by using UV/Vis spectroscopy (Figure S1), dynamic light scattering (DLS), and cryoscopic TEM (Figure 1d, Tables S1–S3, and Figures S8–S12), as well as by inspecting the visual appearance of the dispersions (Figure S2). The micelle core diameters were obtained from TEM images and the hydrodynamic diameters (D_h) were calculated from the DLS measurements.^[33,39] Micelles from Block-1, Block-2, Block-3, and Block-5 were categorized under crew-cut micelles with an exceedingly small corona from the P4VPQ block. Micelles from Block-4, with the longer hydrophilic block, were shown to be star-like micelles (not star-shaped polymers) with a much larger hydrodynamic diameter than the core size (Figure 1d). Schematic illustrations of all five micelles are presented in Figure 1e. The core size of the micelles scaled with the number of PS monomers, by cubic root dependence (Figure 1f), demonstrating a simple space-filling of the core with the non-soluble block. In addition, the star-like micelles (Block-4) followed the same linearity as the crew-cut micelles (Block-1,2,3,5). This was unexpected because the Block-4 micelles had a larger number of charged monomers than the crew-cut micelles. Thus, we expected the core size to decrease because of the increased electrostatic repulsion in the block, as reported for similar amphiphilic block copolymer micelles [i.e., PS-block-poly(acrylic acid)].^[40] Furthermore, the linear dependence of the cubic root of the polystyrene monomer ($n^{1/3}$) on the core diameter suggested that the aggregation number was low ($N_{agg} = 86 \pm 5$). Simplified space-filling calculations provided an estimation of the aggregation number ($N_{agg,av.} = 61 \pm 13$, see the Supporting Information for the calculation details). The slight discrepancy should not be taken as to invalidate the close packing, but to provide an estimate for aggregation number with two separate methods. The low aggregation number also suggested weaker dependence on the diameter of the micelle to the insoluble block than those predicted from scaling theories,^[39,41] which was attributed to the low interfacial tension between the micelle core and the solvent during micellization.^[42] This weak dependence was not surprising because water reportedly “freezes” the block copolymer micelle configuration at low water concentrations,^[38] indicating that micelles are not in dynamic equilibrium with the solution.

The outline of the experimental work is shown in Figure 1g. After the micelles were prepared, they were adsorbed onto fibers or model surfaces (mica) and subsequently heat treated. The adsorption of the micelles on an anionic model substrate (mica) enabled the accurate detection of the micelles without the interference of the substrate roughness. The AFM images revealed a surface fully covered with spherical micelles after the adsorption of the block copolymer micelles, washing with deionized water, and drying (Figure 2). All of the block copolymers adsorbed onto the surface in a closely packed manner and no deviation was observed for the star-like Block-4 micelles.

The hydrophobization of a surface by using amphiphilic block copolymer micelles can be achieved through micellar opening, which exposes the hydrophobic core to the exteri-

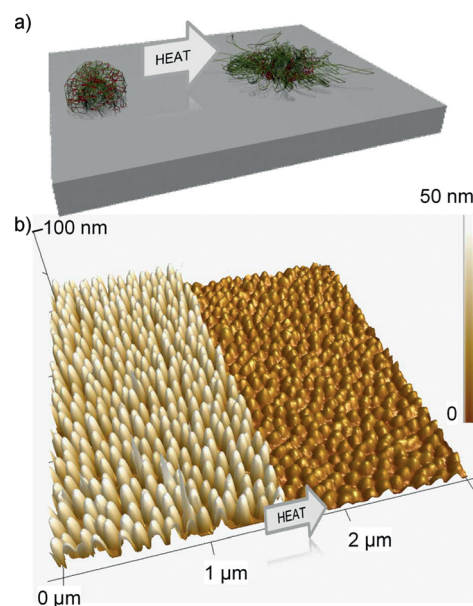


Figure 2. a) An illustration showing the opening of a micelle. b) AFM image of amphiphilic block copolymer micelle (Block-5) on a mica surface before and after heat treatment (see Figure S6 for the AFM images of all samples and Figure S7 in the Supporting Information for 2D images). Note that the height scale in the AFM images is different from the lateral scale, and that the lateral dimensions of the micelles are exaggerated in the AFM because of the tip broadening effect.

or.^[32] To achieve this, we heated the surfaces in an oven (130 °C, 3 min) to open the micelles, which was followed by AFM measurements (Figure 2). The surface was slightly less hydrophilic as the static contact angle of the treated surfaces increased from $\approx 30^\circ$ to $60\text{--}70^\circ$ (Table S5). The static contact angle increase was in agreement with previously published data on model surfaces of silicon oxide.^[32] When the temperature of the heat treatment was above the T_g , the PS fluidized the micelle core and flattened the surface, as suggested by the decrease in height of the micelles in the AFM images (Figure 2).

Upon adsorption of the micelles onto cellulosic fibers, the adsorbed amount increased linearly with the (core) size of the polymer (Figure 3a), as deduced from the cryoscopic TEM images (Figures S8–S12). This suggested that only the surface of the fibers was coated and the micelles did not reach the porous fiber wall. We further characterized the localization of the micelles by using the Raman-imaging technique. Although the resolution of Raman imaging is diffraction limited (≈ 300 nm), it is able to reveal the presence of much smaller micelles. Here, the Raman-imaged fiber cross-section confirmed that only the surface of the fibers had been coated with the micelles (Figure 3b). Adsorption exclusively onto a fibers surface and not into the porous interior has frequently been reported for high molecular weight polyelectrolytes.^[43] This surface selectivity is economical because the micelles are not consumed by the process of adsorption into the interior of the fiber cell walls, which occurs with many low molecular weight polymers adsorbed on cellulosic fibers.^[44,45]

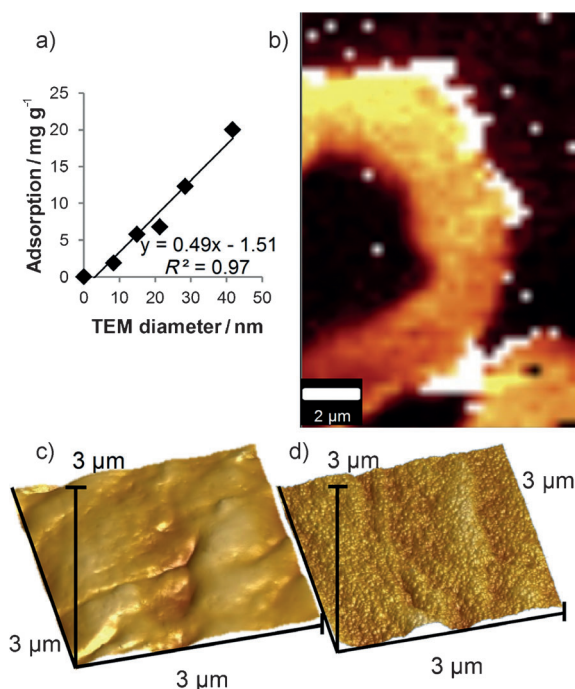


Figure 3. a) The adsorption of different block copolymer micelles on dry cellulosic fibers. The linear correlation suggested that only the surface was coated. b) Cross-sectional Raman imaging of a single fiber, demonstrating the abundance of the micelles on the surface. Cellulose is represented in yellow and Block-5 micelles are white; around one half of a hollow fiber is exposed in the image. c, d) AFM images of Block-5 micelle-treated papers (pseudo-3D image, $3 \times 3 \times 3 \mu\text{m}^3$) for heat treated and room-temperature-dried fiber surfaces, respectively (see Figure S6 for the AFM images of all samples).

The drying of the fibers after adsorption was performed at two distinct temperatures of 25 and at 130 °C, that is, below and above T_g of the amphiphilic block copolymer micelles ($T_g \approx 100^\circ\text{C}$).^[46] Micellar opening of the fibers was observed through AFM images that showed the dotted micellar texture transforming into a smooth surface after treatment at temperatures above T_g (Figure 3c and d). The advancing contact angles of the micelle treated papers are shown in Figure 4a. The samples dried at room temperature that contained low molecular weight block copolymers (Block-1 to Block-3 in Fig-

ure 3b) did not exhibit any significant increase in hydrophobicity. Unexpectedly, however, when the size of the individual micelles reached 30 nm (Block-4 and Block-5), the fiber surfaces became distinctly hydrophobic with advancing water contact angles reaching 120° without heat treatment. These results were in contrast to the model surface measurements, in which only a moderate increase in the water contact angles (up to $\approx 50^\circ$) was observed. The contrast could be ascribed to the significant changes in the fiber texture upon drying.

Micelle adsorption occurs when the fiber is water-swollen, and drying after adsorption shrinks the fiber. As the volume decreases, the surface area of a single fiber can contract as much as 99% during drying.^[47] The shrinkage occurs in the fiber interior, but it also causes an increase in roughness of the fiber surface as the exterior buckles around the shrunken core.^[48] Micelles adsorbed onto the fiber surface undergo a significant rearrangement caused by the roughness increase. When the micelle diameter is large enough ($>30\text{ nm}$), their geometrical constraints result in a rearrangement to form favorable roughness at multiple length scales, which allows for high hydrophobicity to be introduced.

To the best of our knowledge, this study represents the first time that the surface roughening of fibers (a well-known phenomenon in the technical literature of papermaking) has been utilized with a specific physicochemical treatment to reach ultrahydrophobic characteristics. Regrettably, the surface roughening, contrary to the fiber shrinkage, could not be reliably quantified because the AFM images obtained from different locations on the fiber surface were not representative. One could anticipate that future geometrical modeling of heterogeneous fibers would lead to a more quantitative view on the relationship between fiber collapse upon drying and the roughening effect. This would allow a more rigorous treatise on the phenomena behind the hydrophobizing effect.

As expected, elevating the temperature of the micelle-treated fibers to 130 °C transformed the hydrophobicity of nearly all fibers, excluding Block-1 (Figure 4a). The advancing contact angles reached values above 150°. The high contact angles demonstrated the advantage of using block copolymer micelles together with the roughening of the fiber surface to controllably hydrophobize cellulosic fibers. The star-like micelle

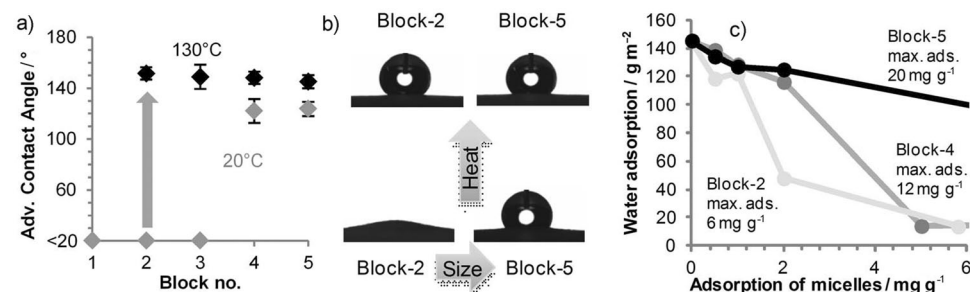


Figure 4. a) The effect of heating on block copolymer adsorption, and subsequent heating to the hydrophobization of paper (all contact angle values are listed in Table S4). b) Images of the actual water droplets on the paper, which schematically shows the effect of both heat and the micelle size to the hydrophobization effect. c) Water absorption on heat-treated paper samples as a function of the adsorbed amount block copolymer micelles. The associated error of the measurement was approximately 5%.

(Block-4) with a longer hydrophilic block followed the same tendency as the other micelles. This demonstrated that the hydrophobizing effect of our block copolymer micelles did not depend on the size of the micelle in the aqueous state (hydrodynamic diameter), but solely upon the core size of the micelle. AFM images showed a smooth continuous coating, which closely followed the roughness of the fibrillar surface without distinctive micellar features (Figure 3c and Figure S6 in

the Supporting Information). In contrast to the high advancing contact angles, the receding angles were very low ($<20^\circ$). The large contact angle hysteresis denoted “sticky” hydrophobicity; the hydrophobicity attained with high hysteresis could be termed as adhesive ultrahydrophobicity.^[49–52] This is the opposite of the self-cleaning “lotus-effect” in which the water droplets spontaneously roll off from the surface because of minimal hysteresis coupled with $>150^\circ$ water contact angles.^[53]

Figure 4b illustrates the absorption of water into paper that was produced from block copolymer treated fibers with heat treatment at 130°C . The water absorption is depicted as a function of the adsorbed amount of the block copolymer micelles. It appeared that the addition of micelles of approximately one third of their maximum adsorption on the fibers was enough to significantly suppress the water absorption.

Conclusions

In summary, after adsorption of amphiphilic block copolymer micelles, the well-reported microscopic shrinking of cellulosic fibers upon drying results in favorable rearrangements in the larger micelles. This results in an increase in the advancing water contact angles of the fibers up to $\approx 130^\circ$. Mild heating (130°C) causes further exposure of the hydrophobic block within the micelles, leading to high adhesive hydrophobicity with advancing contact angles exceeding 150° . The amphiphilic block copolymer micelles with hydrophobized surfaces have the potential to be used for state-of-the-art systems in which hydrophobization and/or contact with synthetic polymers are required.

Experimental Section

Materials: The fibers used were commercial elemental chlorine free (ECF) bleached birch kraft pulp produced in Botnia, Äänekoski, Finland. The fibers consisted primarily of cellulose ($\approx 70\%$) and xylan ($\approx 30\%$), as shown by detailed characterization in our previous work.^[54] To maximize the homogeneity, the small fiber section (called fines) was removed^[44] and the counter-ions of the carboxylic acid moieties were exchanged to Na^+ .^[55] Several PS-*b*-P4VPQ block copolymers were obtained from PolymerSource Inc. (Montreal, Canada). Micellation of the block copolymers was performed according to the procedure detailed by Gao et al.^[33]

Methods: A CAM-200 contact angle goniometer (KSV Instruments Ltd, Helsinki, Finland) was used to measure the dynamic (advancing and receding) contact angle through the embedded needle method (Figure S13). DLS with a Zetasizer Nano90 Instrument (Malvern Instruments, Worcestershire, UK) was used to determine the hydrodynamic diameter. AFM images were taken with a Nanoscope IIIa Multimode scanning probe microscope (Digital Instruments Inc., Santa Barbara, CA, USA) equipped with J-scanner. Epoxy resin embedded samples were analyzed with an alpha300 R confocal raman microscope (Witec GmbH, Germany) under ambient conditions; the results were analyzed with WiTec Project 1.94 software (WiTec GmbH, Germany, see Figures S3–S5). The cryoscopic TEM samples were loaded onto carbon grids and measured with a 300 kV transmission electron microscope (JEOL JEM-3200FSC, Japan) operated at liquid helium temperature. The TEM image analysis was performed in the Anduril pipeline framework,^[56] and

we implemented the spherical feature scale detection as introduced by Lindeberg.^[57] The water adsorption of the amphiphilic micelle-treated papers was conducted for heat-treated samples by using a standard method (SCAN-P 12:64). In short, water was poured on sample paper with a known surface area and after 30 s the adsorbed water was measured. The results were detailed as $g_{\text{water}} m_{\text{paper}}^{-2}$. A detailed description of the experimental procedures is provided in the Supporting Information (Raman imaging is shown in Figures S3–S5, the tabulated results are detailed in Tables S1–S3, and TEM image analysis is provided in Figures S8–S12).

Acknowledgements

We thank Ritva Kivelä for obtaining the AFM images. Botnia, Kemira, UPM, Andritz, and the Finnish Centre for Technology and Innovation (TEKES) are thanked for financing through the Chemically Aided Drying project (ChAD).

Keywords: adsorption • block copolymers • hydrophobic effect • micelles • surface chemistry

- [1] R. Pelton, *TrAC Trends Anal. Chem.* **2009**, *28*, 925–942.
- [2] P. J. Bracher, M. Gupta, G. M. Whitesides, *Soft Matter* **2010**, *6*, 4303–4309.
- [3] D. Tobjörk, R. Österbacka, *Adv. Mater.* **2011**, *23*, 1935–1961.
- [4] A. W. Martinez, S. T. Phillips, G. M. Whitesides, E. Carrilho, *Anal. Chem.* **2010**, *82*, 3–10.
- [5] H. Orelma, I. Filpponen, L.-S. Johansson, J. Laine, O. J. Rojas, *Biomacromolecules* **2011**, *12*, 4311–4318.
- [6] H. Orelma, T. Teerinen, L.-S. Johansson, S. Holappa, J. Laine, *Biomacromolecules* **2012**, *13*, 1051–1058.
- [7] A. Yu, J. Shang, F. Cheng, B. A. Paik, J. M. Kaplan, R. B. Andrade, D. M. Ratner, *Langmuir* **2012**, *28*, 11265–11273.
- [8] J. Lankelma, Z. Nie, E. Carrilho, G. M. Whitesides, *Anal. Chem.* **2012**, *84*, 4147–4152.
- [9] S. J. Vella, P. Beattie, R. Cademartiri, A. Laromaine, A. W. Martinez, S. T. Phillips, K. A. Mirica, G. M. Whitesides, *Anal. Chem.* **2012**, *84*, 2883–2891.
- [10] A. C. Araújo, Y. Song, J. Lundberg, P. L. Ståhl, H. Brumer, *Anal. Chem.* **2012**, *84*, 3311–3317.
- [11] Y. J. Kang, H. Chung, C.-H. Han, W. Kim, *Nanotechnology* **2012**, *23*, 289501.
- [12] W. Zhang, X. Zhang, C. Lu, Y. Wang, Y. Deng, *J. Phys. Chem. C* **2012**, *116*, 9227–9234.
- [13] P. Barquinha, R. Martins, L. Pereira, E. Fortunato, *Transparent Oxide Electronics*, Wiley, Chichester, UK, **2012**.
- [14] L. Hu, J. W. Choi, Y. Yang, S. Jeong, F. La Mantia, L.-F. Cui, Y. Cui, *Proc. Natl. Acad. Sci. USA* **2009**, *106*, 21490–21494.
- [15] A. G. Avila, J. P. Hinstroza, *Nat. Nanotechnol.* **2008**, *3*, 458–459.
- [16] G. Yu, L. Hu, M. Vosgueritchian, H. Wang, X. Xie, J. R. McDonough, X. Cui, Y. Cui, Z. Bao, *Nano Lett.* **2011**, *11*, 2905–2911.
- [17] Y. Liu, X. Wang, K. Qi, J. H. Xin, *J. Mater. Chem.* **2008**, *18*, 3454.
- [18] L. Bao, X. Li, *Adv. Mater.* **2012**, *24*, 3246–3252.
- [19] W. Zhao, M. M. Ali, S. D. Aguirre, M. A. Brook, Y. Li, *Anal. Chem.* **2008**, *80*, 8431–8437.
- [20] M. A. Hubbe, H. Nanko, M. R. McNeal, *BioResources* **2006**, *2*, 106–145.
- [21] T. Lindström, P. T. Larsson, *Nord. Pulp Pap. Res. J.* **2008**, *23*, 202.
- [22] J. Lindfors, S. Ahola, T. Kallio, J. Laine, P. Stenius, M. Danielsson, *Nord. Pulp Pap. Res. J.* **2005**, *20*, 453–458.
- [23] F. Eder, H. Klauk, M. Halik, U. Zschieschang, G. Schmid, C. Dehm, *Appl. Phys. Lett.* **2004**, *84*, 2673.
- [24] D.-H. Kim, Y.-S. Kim, J. Wu, Z. Liu, J. Song, H.-S. Kim, Y. Y. Huang, K.-C. Hwang, J. A. Rogers, *Adv. Mater.* **2009**, *21*, 3703–3707.
- [25] R. Bollström, A. Määttä, D. Tobjörk, P. Ihalainen, N. Kaihovirta, R. Österbacka, J. Peltonen, M. Toivakka, *Org. Electron.* **2009**, *10*, 1020–1023.
- [26] B. P. Andersson, D. Nilsson, P.-O. Svensson, M. Chen, A. Malmström, T. Remonen, *Adv. Mater.* **2002**, *14*, 1460–1464.

- [27] J. Olkkonen, K. Lehtinen, T. Erho, *Anal. Chem.* **2010**, *82*, 10246–10250.
- [28] E. Carrilho, A. W. Martinez, G. M. Whitesides, *Anal. Chem.* **2009**, *81*, 7091–7095.
- [29] R. Vyhnalkova, A. Eisenberg, T. van de Ven, *Macromol. Biosci.* **2011**, *11*, 639–651.
- [30] M. A. Hubbe, R. A. Venditti, O. J. Rojas, *BioResources* **2007**, *2*, 739–788.
- [31] S. Utsel, E. E. Malmström, A. Carlmark, L. Wågberg, *Soft Matter* **2010**, *6*, 342.
- [32] S. Utsel, A. Carlmark, T. Pettersson, M. Bergström, E. E. Malmström, L. Wågberg, *Eur. Polym. J.* **2012**, *48*, 1195–1204.
- [33] Z. Gao, S. K. Varshney, S. Wong, A. Eisenberg, *Macromolecules* **1994**, *27*, 7923–7927.
- [34] J. Gouin, F. Bosse, D. Nguyen, C. Williams, A. Eisenberg, *Macromol. Symp.* **1993**, *26*, 7250–7255.
- [35] K. Khougaz, Z. Gao, A. Eisenberg, *Macromolecules* **1994**, *27*, 6341–6346.
- [36] I. Astafieva, X. F. Zhong, A. Eisenberg, *Macromolecules* **1993**, *26*, 7339–7352.
- [37] D. Nguyen, S. K. Varshney, C. E. Williams, A. Eisenberg, *Macromolecules* **1994**, *27*, 5086–5089.
- [38] L. Zhang, H. Shen, A. Eisenberg, *Macromolecules* **1997**, *30*, 1001–1011.
- [39] M. Moffitt, K. Khougaz, A. Eisenberg, *Acc. Chem. Res.* **1996**, *29*, 95–102.
- [40] L. Zhang, A. Eisenberg, *J. Am. Chem. Soc.* **1996**, *118*, 3168–3181.
- [41] S. Förster, V. Abetz, A. H. E. Miiller, *Adv. Polym. Sci.* **2004**, *166*, 173–210.
- [42] L. Zhang, K. Khougaz, M. Moffitt, A. Eisenberg in *Amphiphilic Block Copolymers: Self-Assembly and Applications (Studies in Surface Science and Catalysis)* (Eds.: P. Alexandridis, B. Lindman), Elsevier Science Ltd, **2000**, pp. 87–113.
- [43] A. T. Horvath, A. E. Horvath, T. Lindström, L. Wågberg, *Langmuir* **2008**, *24*, 10797–10806.
- [44] A. T. Horvath, A. E. Horvath, T. Lindström, L. Wågberg, *Langmuir* **2008**, *24*, 6585–6594.
- [45] A. T. Horvath, A. E. Horvath, T. Lindström, L. Wågberg, *Langmuir* **2008**, *24*, 7857–7866.
- [46] L. Zhang, A. Eisenberg, *Science* **1995**, *268*, 1728–1731.
- [47] J. E. Stone, A. M. Scallan, G. M. A. Aberson, *Pulp Pap. Mag. Can.* **1966**, *67*, 263–268.
- [48] H. G. Higgins, A. W. McKenzie, *Appita* **1963**, *16*, 145–164.
- [49] J. N. Mateo, S. S. Kulkarni, L. Das, S. Bandyopadhyay, G. C. Tepper, K. J. Wynne, S. Bandyopadhyay, *Nanotechnology* **2011**, *22*, 035703.
- [50] H. Jin, M. Kettunen, A. Laiho, H. Pynnönen, J. Paltakari, A. Marmur, O. Ikkala, R. H. A. Ras, *Langmuir* **2011**, *27*, 1930–1934.
- [51] K.-H. Cho, L.-J. Chen, *Nanotechnology* **2011**, *22*, 445706.
- [52] L. Taajamaa, E. Kontturi, J. Laine, O. J. Rojas, *J. Mater. Chem.* **2012**, *22*, 12072.
- [53] D. Quéré, M. Reyssat, *Philos. Trans. R. Soc. London Ser. A* **2008**, *366*, 1539–1556.
- [54] N. Aarne, E. Kontturi, J. Laine, *Soft Matter* **2012**, *8*, 4740.
- [55] L. Wågberg, L. Ödberg, G. Glad-Nordmark, *Nord. Pulp Pap. Res. J.* **1989**, *4*, 71.
- [56] K. Ovaska, M. Laakso, S. Haapa-Paananen, R. Louhimo, P. Chen, V. Aittomäki, E. Valo, J. Núñez-Fontarnau, V. Rantanen, S. Karinen, K. Nousiainen, A.-M. Lahesmaa-Korpinen, M. Miettinen, L. Saarinen, P. Kohonen, J. Wu, J. Westermarck, S. Hautaniemi, *Genome Med.* **2010**, *2*, 65.
- [57] T. Lindeberg, *Int. J. Comput. Vis.* **1998**, *30*, 79–116.

Received: March 9, 2013

Published online on May 17, 2013

Supporting Information

© Copyright Wiley-VCH Verlag GmbH & Co. KGaA, 69451 Weinheim, 2013

Controlled Hydrophobic Functionalization of Natural Fibers through Self-Assembly of Amphiphilic Diblock Copolymer Micelles

Niko Aarne,^[a] Janne Laine,^[a] Tuomas Hänninen,^[b] Ville Rantanen,^[c] Jani Seitsonen,^[d]
Janne Ruokolainen,^[d] and Eero Kontturi*^[a]

cssc_201300218_sm_miscellaneous_information.pdf

Supporting Information Table of Contents

Supporting Information Table of Contents	S1
S1. Detailed experimental information	S1
S1.1. Fiber properties	S1
S1.2. Block copolymer properties	S1
S1.3. Micellation of the block copolymers	S2
S1.4. Adsorption of micelles on cellulosic fibers.....	S2
S1.5. Light Scattering analysis.....	S2
S1.6. AFM imaging.....	S2
S1.7. Raman imaging	S2
S1.8. TEM imaging	S3
S1.9. TEM Image analysis	S3
S1.10. Contact angle measurements.....	S3
S1.11. Water adsorption measurements	S4
S2. Calculations.....	S4
S2.1. Calculation of the aggregation numbers N_{agg}	S4
S3. UV-vis spectroscopy	S6
S4. RAMAN spectroscopy and imaging.....	S7
S5. AFM imaging.....	S9
S6. TEM images and image analysis results	S11
S7. Dynamic light scattering data	S14
S8. Contact angles	S15
REFERENCES.....	S16

S1. Detailed experimental information

S1.1. Fiber properties

The fibers used were commercial elemental chlorine free (ECF) bleached birch kraft pulp produced in Botnia, Äänekoski, Finland. The smallest fiber section (fines) was removed through 200 mesh (PF-305 Poremet, G. Bopp + Co. AG, Zurich, Germany) at constant consistency (6.0 g/L) maintained by 5.0 L/min tap water (conductivity $\sim 200 \mu\text{S}/\text{cm}$) in a large 200 L container. The method was adapted from SCAN-M 6:69 standard. The counter-ions of the carboxylic groups in the fibers were converted to sodium (Na-form) by a standard practice[S1]. In short, the fibers were immersed to a 10 mM HCl solution (8-10 g/L) for 30 min, filtrated and washed with deionized water until the conductivity was $< 5 \mu\text{S}/\text{cm}$. This converted the carboxylic groups to their protonated form. Finally, the fibers were mixed for 30 min in 5mM NaHCO_3 solution, where the pH was adjusted to 8-9 with 1 M NaOH. Filtration and washing until conductivity was $< 5 \mu\text{S}/\text{cm}$ resulted in the Na-form fibers.

S1.2. Block copolymer properties

Several polystyrene-*block*-poly(*N*-methyl-4-vinyl pyridinium iodide) block copolymers were obtained from PolymerSource Inc. (Montreal, Canada). We used the polymers as received, due to the extensive characterization given upon purchasing the material: The company provided the polydispersity and molecular weight data based on size exclusion

chromatography and the company confirmed the complete quaternatization by the disappearance of the pyridine band at 1412 cm^{-1} in FT-IR spectrum.

S1.3. Micellation of the block copolymers

Micellation was done according to the procedure described in detail by Gao *et al.*[S2]. In short, approximately 0.5 g were mixed in 10 g dimethylformamide (DMF, analytical grade, Sigma Aldrich) until dissolved (~24 h). The solutions were filtered through Whatman 541 filter paper (GE Healthcare, USA) to remove any undissolved particles. Subsequently, water (MilliQ, conductivity $0.5\text{ }\mu\text{S/cm}^{-1}$) was slowly added from a peristaltic pump adjusted to 0.25 mL/min, until the solution reached volume of approx. 100 mL. The micellar solutions were dialyzed against distilled water for 3 days in continuous flow dialysis equipment. We used Spectra/Por dialysis tubes of 6000 M_w cut-off (Spectrum Europe B.V., Breda, The Netherlands). Finally, the solution concentration was determined by drying three ~1 g samples in oven ($105\text{ }^{\circ}\text{C}$).

S1.4. Adsorption of micelles on cellulosic fibers

The block copolymer micelles were adsorbed to the Na-form fibers (6.0 g/L consistency) in 1 mM NaHCO_3 buffer. The buffer use is a standard practice to avoid the pH decrease, which might affect the adsorption due to pH falling near the pK_a of carboxylic acids in the pulp. The adsorption was determined with UV-VIS spectrometer (Shimadzu UV-2550, Shimadzu Corporation, Tokyo, Japan) from the decreasing shoulder at 255 nm, originating from the aromatic moieties in polystyrene-*block*-poly(*N*-methyl-4-vinyl pyridinium iodide) ions in water (Figure S1). UV-Vis calibration curves were done to verify the absorption dependence on concentration (Figure S1 inset). We also show the faint colors of the solutions (Figure S2), since the faint absorption in the VIS-region above 400 nm is not visible in the spectra (Figure S1).

S1.5. Light Scattering analysis

The hydrodynamic diameter was determined by Dynamic Light Scattering (DLS) using a Zetasizer Nano90 Instrument (Malvern Instruments, Worcestershire, UK) equipped with a 4 mW He-Ne laser (633 nm wavelength). The scattering angle used for the measurements was 90° and the Stokes-Einstein equation was used to convert the diffusion coefficient into hydrodynamic diameter (D_h). The Z-average size calculations were automatically done according to standards: ISO 13321 and ISO 22412. The micellar solutions were filtered through $1.0\text{ }\mu\text{m}$ filters (Acrodisk® CR, PTFE membrane, Pall Life Sciences, Ann Arbor, MI, USA) before analysis.

S1.6. AFM imaging

AFM images were taken with a Nanoscope IIIa Multimode scanning probe microscope (Digital Instruments Inc., Santa Barbara, CA, USA) equipped with J-scanner. The images were scanned in tapping mode with NSC15/AIBS tips (Ultrasharp μmasch , Tallinn, Estonia) with measured resonance frequency of $280\pm 10\text{ kHz}$. Typical force constants were $46\pm 25\text{ N/m}$ and the radius of curvature of the tips was $<10\text{ nm}$, as reported by the manufacturer.

S1.7. Raman imaging

Pulp sheet samples were embedded in epoxy resin (Agar Low Viscosity Resin, Agar scientific, Essex, England) under vacuum and cured overnight before sectioning. Epoxy blocks were sectioned using a razor blade to obtain smooth surface for Raman imaging. Samples were

analyzed with an alpha300 R Confocal Raman microscope (Witec GmbH, Germany, www.witec.de) at ambient conditions. The Raman spectra were obtained by using a frequency doubled Nd:YAG laser (532.35 nm, 10 mW) and a Nikon 100× (NA=0.95) air objective. The Raman system was equipped with a DU970N-BV EMCCD camera behind a 600 lines/mm grating. The excitation laser was polarized horizontally. For each Raman image, an integration time and excitation laser power was varied depending on how prone the samples were to burn. The size of one pixel in the image was 0.33 μm . The baselines of the spectra were corrected with WiTec Project 1.94 (WiTec GmbH, Germany, www.witec.de) by employing a fifth order equation using wavenumber regions presented in Figure S3. For the Raman-image, the chosen wavenumbers were 999-1006 cm^{-1} for the block copolymer (characteristic for styrene aromatic C-C stretching), 1090-1100 cm^{-1} for the fiber cell wall (characteristic for cellulose C-O stretch) and 1719-1760 cm^{-1} for the epoxy resin (Figure S4).

S1.8. TEM imaging

Cryo-Transmission Electron Microscopy (cryo-TEM) was carried out using field emission cryo-electron microscope (JEOL JEM-3200FSC, JEOL Ltd., Tokyo, Japan), which was operating at 300 kV voltage. Images were taken in bright field mode and using zero loss energy filtering (omega type) with the slit width of 20 eV. Micrographs were recorded using Gatan Ultrascan 4000 CCD camera (Gatan Inc., Pleasanton, CA, USA). Specimen temperature was maintained at -255 °C during the imaging. Vitrified specimens were prepared using automated FEI Vitrobot device (FEI Company, Hillsboro, OR, USA) using Quantifoil 3.5/1 holey carbon copper grids (Quantifoil Micro Tools GmbH, Jena, Germany) with the hole size of 3.5 μm . Just prior to use grids were plasma cleaned by Gatan Solarus 9500 plasma cleaner (Gatan Inc., Pleasanton, CA, USA) and then transferred into an environmental chamber of FEI Vitrobot having room temperature and 100 % humidity. Thereafter 3 μl of sample solution was applied on the grid and the sample was blotted once for 1 seconds and then vitrified in 1/1 mixture of liquid ethane and propane at temperature of -180 °C. The grid with vitrified sample solution were maintained at liquid nitrogen temperature and then cryo-transferred in to the microscope.

S1.9. TEM Image analysis

The TEM image analysis was carried out in the pipeline framework Anduril[S3]. To measure the sizes of the amphiphilic block copolymer micelle we created a pipeline to detect round image features at different scales. For the detection, we implemented spherical feature scale detection as introduced by Lindeberg[S4]. The detection is semi-automatic, or visually guided, to improve detection accuracy. For each group of expected sizes, we guided the algorithm to find objects at an expected size range. In addition, the algorithm was more accurate with spherical features that had two radii (i.e. ovals). From the two radii, the shorter one corresponded to the actual radius of the micelle and was identified as micelle radius. The tabulated results as well visualizations of the feature detection are reported in Table S2 and Figure S8-Figure S12).

S1.10. Contact angle measurements

CAM-200 contact angle goniometer (KSV Instruments Ltd, Helsinki, Finland) was used to measure the dynamic contact angle with the embedded needle method. We also measured the contact angle (CA) with the sessile drop method. The results are tabulated in Tables S3-S4 and an example of the dynamic contact angle measurement is shown in Figure S13.

S1.11. Water adsorption measurements

The water adsorption of the amphiphilic micelle treated papers was conducted for heat-treated samples. COBB test (SCAN-P 12:64) was used to measure water adsorption. It is a standardized method to determine water adsorption in our field. We used a shorter time period of 30 second to obtain sensible value for untreated reference, since the method is mainly used for paperboards and other hydrophobized paper products. (The standard soaking period of 60 seconds resulted in disintegration of the paper for the untreated reference paper.) Error of the measurement is approx. 5 %.

S2. Calculations

S2.1. Calculation of the aggregation numbers N_{agg}

The total volume according to the simple space filling of a substance is given by the equation:

$$V_{tot} = N_{agg} \cdot V_{unimer} \quad (S1)$$

where V_{tot} is the total volume, N_{agg} is the aggregation number and V_{unimer} is the volume of a single unimer. The V_{unimer} is further composed of N , the number of monomers, and $V_{monomer}$, the monomer volume:

$$V_{unimer} = N \cdot V_{monomer} \quad (S2)$$

Furthermore, the volumes can be defined to be cubes with side length of d_i . Taking this into account and substituting (S2) to (S1) gives (we ignore the packing factor and assume perfect fitting):

$$d_{tot} = N_{agg}^{1/3} \cdot d_{monomer} \quad (S3)$$

where d_{tot} is the aggregate diameter and $d_{monomer}$ is the monomer diameter. The plot of d_{tot} against $N_{agg}^{1/3}$ gives the slope coefficient as:

$$k = N_{agg}^{1/3} \cdot d_{monomer} \quad (S4)$$

The aggregation number can be then calculated from the slope coefficient in TEM diameter vs. $N_{PS}^{1/3}$ plot (Figure 1f) by the following equation:

$$N_{agg} = \left(\frac{k}{2a} \right)^3 = \left(\frac{k}{d_{monomer}} \right)^3 \quad (S5)$$

where N_{agg} is the aggregation number, k is the slope coefficient and a is the radius of polystyrene monomer. The radius was calculated from the density of the polystyrene according to the equation:

$$a = \frac{d_{monomer}}{2} = \sqrt[3]{\left(\frac{m_{PS-block}}{N_a \cdot N_{PS-block} \cdot \rho_{PS}} \right)} \cdot \frac{3}{4\pi} \quad (S6)$$

where $m_{PS-block}$ is the molecular weight of the styrene-block given by the manufacturer, N_a is the Avogadro's constant, $N_{PS-block}$ the number of monomers in the polymer given by the manufacturer and finally ρ_{PS} is the density of polystyrene. We used 1050 kg/m³ as the density of polystyrene. Eq. S6 gives the maximum diameter estimate for the polystyrene monomer and is only a rough estimate for the diameter (From Eq S6, $d_{monomer}=0.68$). With $k=3.01$ and $a=0.34$ nm and using equation S5 we obtained $N_{agg} = 86$.

Another method to obtain the aggregation number is to use the direct calculation involving volume of the spherical micelle and the unimer volume, both of which can be calculated. A simple division of the volume of the micellar core with the volume of the core constituent (polystyrene) gives the aggregation number:

$$N_{agg} = \frac{V_{tot}}{V_{PS-block}} = \frac{\frac{4\pi}{3} \left(\frac{d_{core}}{2} \right)^3}{\frac{4\pi}{3} (a^3 \cdot N_{PS})} = \frac{d_{core}^3}{d_{PS-monomer}^3 N_{PS-block}} \quad (S7)$$

where N_{agg} is the aggregation number, V_{tot} is the total volume, N_{agg} is the aggregation number and $V_{PS-block}$ is the volume of a polystyrene block in one block copolymer, d_{core} is the polystyrene core diameter obtained from TEM measurements, a is the diameter of styrene monomer determined from Eq. S6. The results are shown in Table S1. Note that none of the block copolymer micelles have the aggregation number determined from Eq. S5. This is due to the different approach taken into calculating the values. The Eq. S5 is a rough approximation based on the linearity found with $n^{1/3}$, while Eq. S7 is a more correct approximation using volume differences. Both approximations ignore complications such as packing and are based on a diameter value for styrene. Better results could be obtained by measuring the average polystyrene monomer size and taking packing into account. These values are difficult to obtain and add little to the article. Therefore, we settled on these approximations that clearly show the low aggregation number of the micelles.

Table S1. Tabulated information from the block copolymers and the block copolymer micelles used in the study. Micelle core diameter (*Diameter*), polystyrene molecular weight (*PS[kDa]*), *N*-methyl-4-vinyl pyridinium iodide molecular weight (*P4VPQ[kDa]*), total molecular weight (*Tot. M_w*), number of polystyrene monomers (*PS[n]*), number of *N*-methyl-4-vinyl pyridinium iodide monomers (*P4VPQ[m]*), adsorption on cellulosic fiber (*Ads.*), radius of the polystyrene monomer (*a*) and aggregation number (N_{agg}).

	Diameter [nm]	PS[a] [kDa]	P4VPQ[a] [kDa]	Tot. M _w [kDa]	PS[b] [n]	P4VPQ[b] [m]	Ads. [mg/g][c]	a[d] [nm]	N _{agg} [e,f] [n]
Block-1	8.4	3.3	11.2	14.5	32	45	1.9	0.34	58
Block-2	14.8	25	16	41.0	240	65	5.8	0.34	43
Block-3	21.3	50	14	64.0	480	57	6.8	0.34	64
Block-4	28.4	122	51	173	1172	206	12.3	0.34	62
Block-5	41.8	310	23.5	334	2979	95	20.0	0.34	78

[a] Molecular weight, given by the manufacturer [b] number of monomers, calculated value from the M_w [c] Adsorbed amount for cellulosic fibers [d] calculated value from eq. S6 [e] calculated value from eq. S7 [f] The value for N_{agg} from eq. S5 is 86.

S3. UV-vis spectroscopy

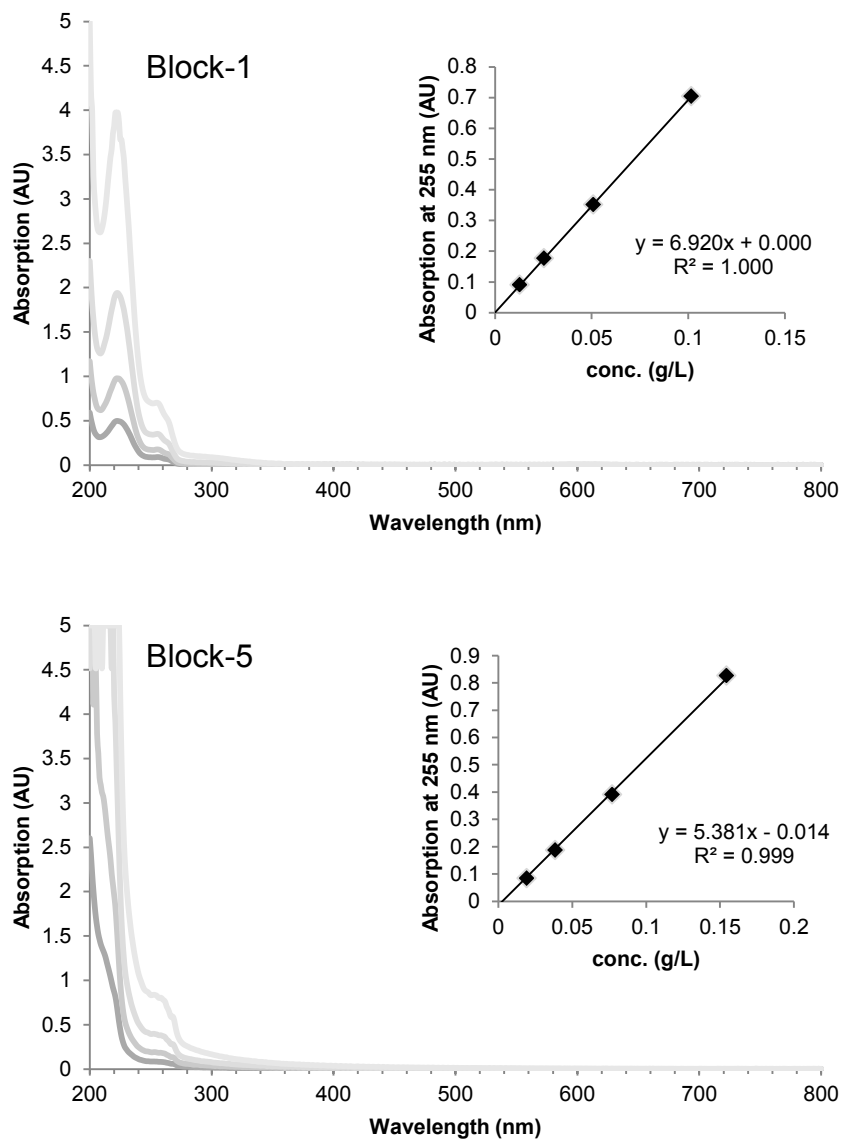


Figure S1. The absorption spectra of two block copolymer micelle solutions. (Above) Block-1 was the solution with largest fraction of pyridine. (Below) Block-5 was the solution with smallest fraction of pyridine. The insets show the linear dependence of the signal at 255 nm. The concentrations in the spectra correspond to those shown in insets.

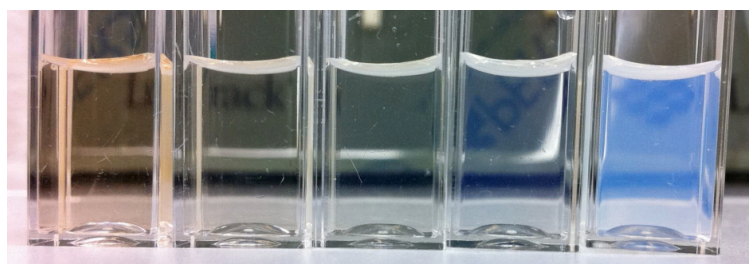


Figure S2. The colored solutions of the block copolymer micelles. From left to right: Block-1, Block-2, Block-3, Block-4 and Block-5.

S4. RAMAN spectroscopy and imaging

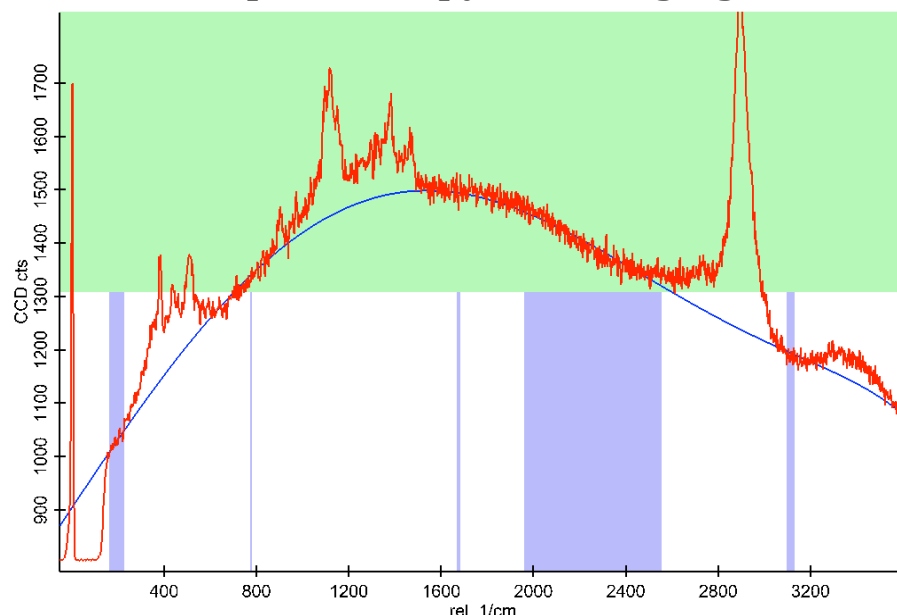


Figure S3. Background removal parameters for Raman imaging. A fifth order equation was used to subtract the background (blue line). The indicated regions (blue rectangles) were used for this equation.

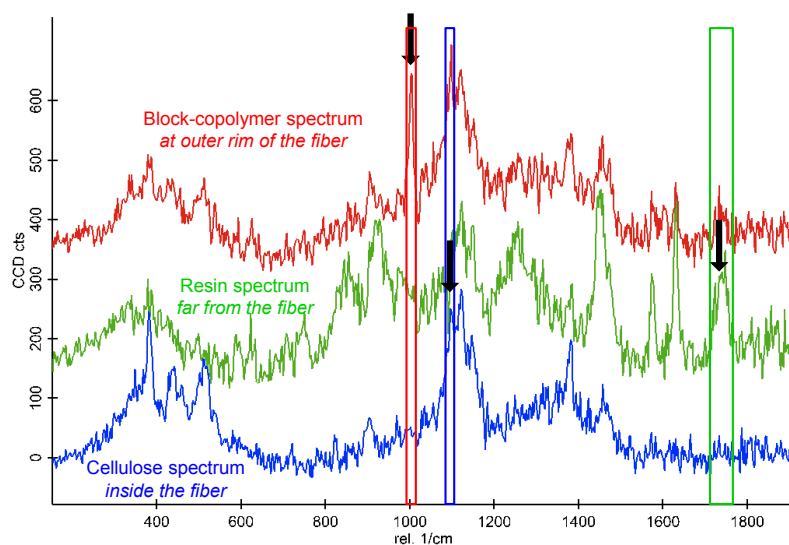


Figure S4. Characteristic spectra of the substances in amphiphilic block copolymer treated fiber. The upmost spectrum was taken at the outer rim of the fiber and shows a characteristic peak at 1000 cm^{-1} . The middle spectrum was taken far from the fiber and represents the resin used to prepare the cross-section. The bottom spectrum was taken from inside the fiber. The characteristic cellulose peak at 1100 cm^{-1} was used to pinpoint the location of cellulose inside the fiber. The resin spectrum could be identified due to the characteristic adsorption at $\sim 1750\text{ cm}^{-1}$.

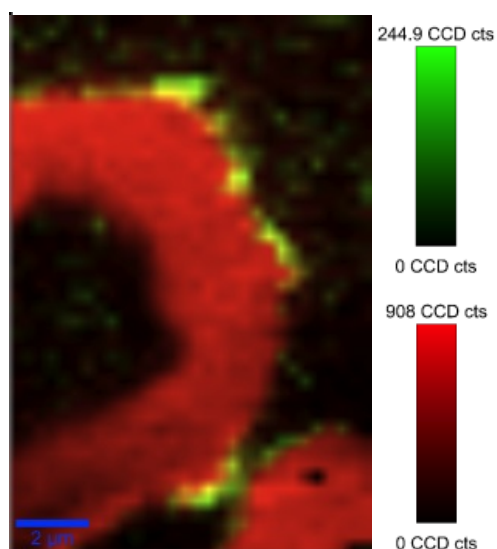


Figure S5. Raman image of fiber cross-section from the area indicated as a white rectangle in micrograph. Green and red colors in the image represent polystyrene and cellulose, respectively.

S5. AFM imaging

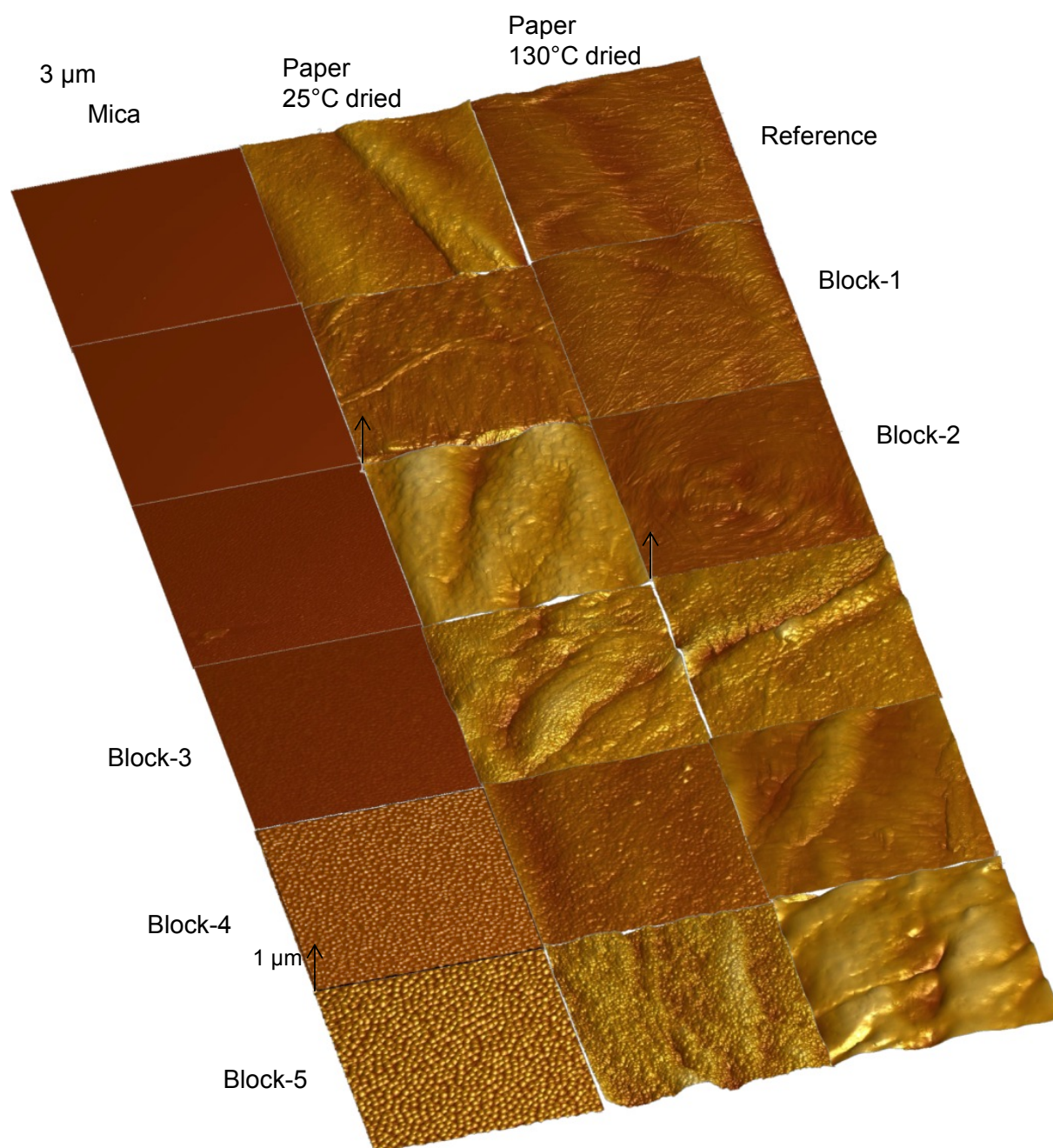
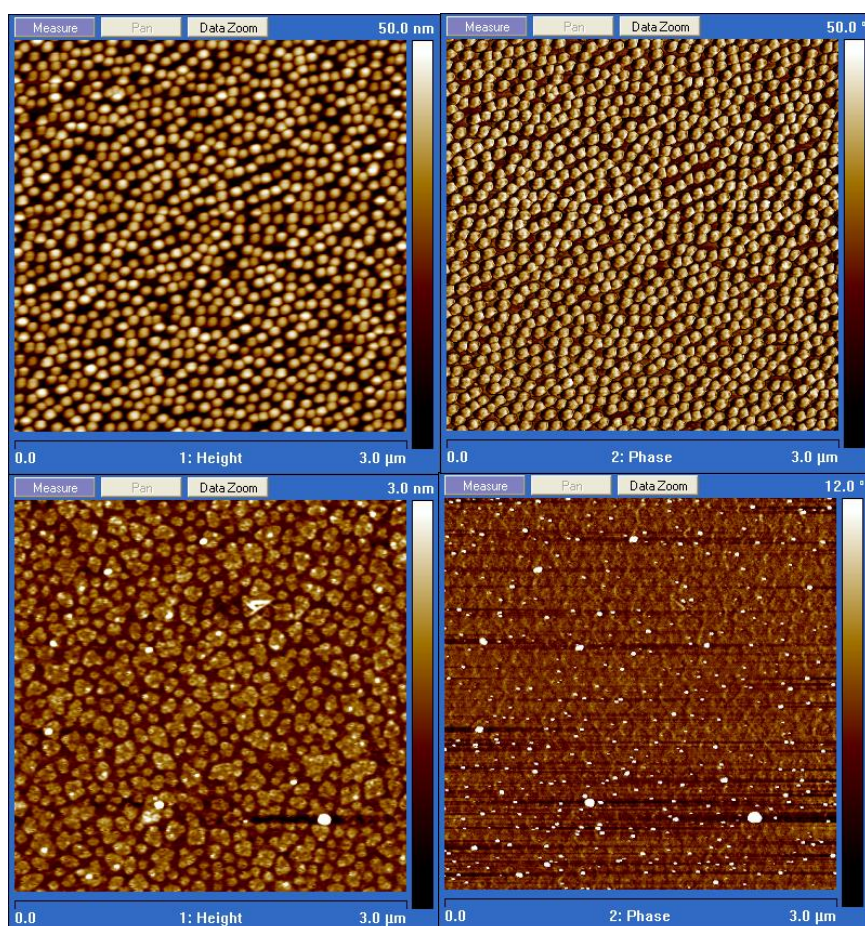


Figure S6. AFM images of the block copolymers. The images are in (pseudo) 3D to demonstrate the qualitative differences between the different block copolymer micelles and between the different drying treatments. The lateral size of all images is $3 \times 3 \times 3 \mu\text{m}^3$. The top row demonstrates the images of reference surfaces (bare mica and non-treated paper). The left column represents the block copolymers from the smallest (Block-1) to largest (Block-5). Middle column shows the surfaces of the papers dried at room temperature. Finally, the rightmost column presents images of the heat-treated papers. Note that the micellar features are clearly visible (e.g. two lowest rows in the figure) until they disappear after the heat treatment. Note: The colors are not to scale.



BLOCK-5
on mica

BLOCK-5
on mica
after heat
treatment

Figure S7. AFM images for block-5 on model substrate before and after heat treatment. (Left) Height images (Right) Angle images.

S6. TEM images and image analysis results

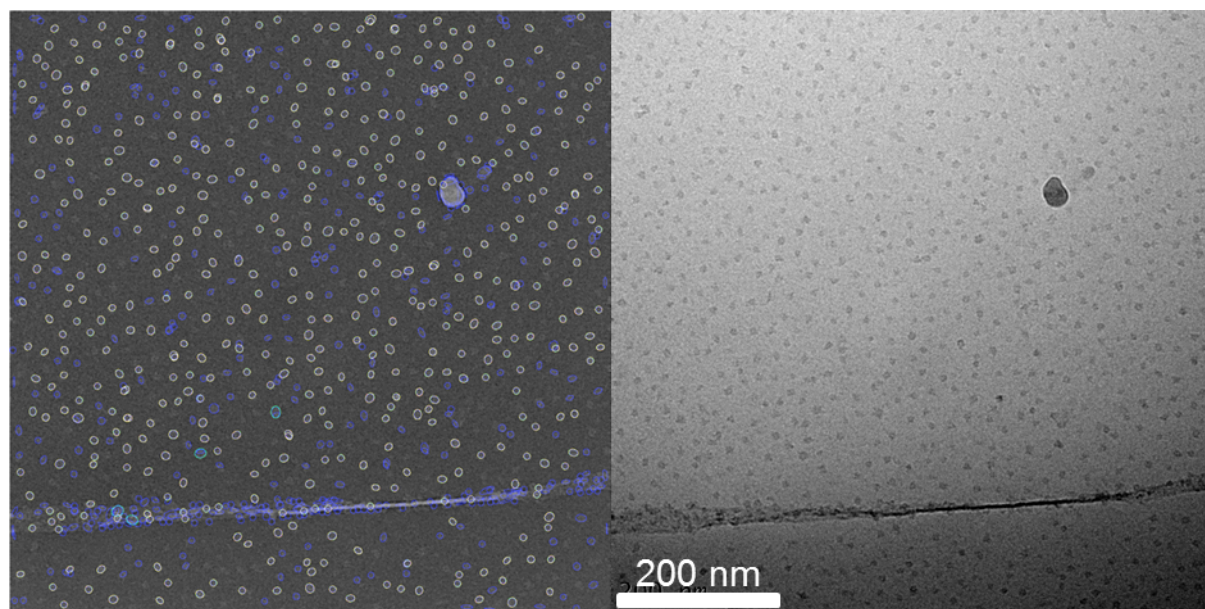


Figure S8. Block-1 micelles as identified by image analysis (left) and as obtained from TEM (right). The blue ovals are rejected micelles.

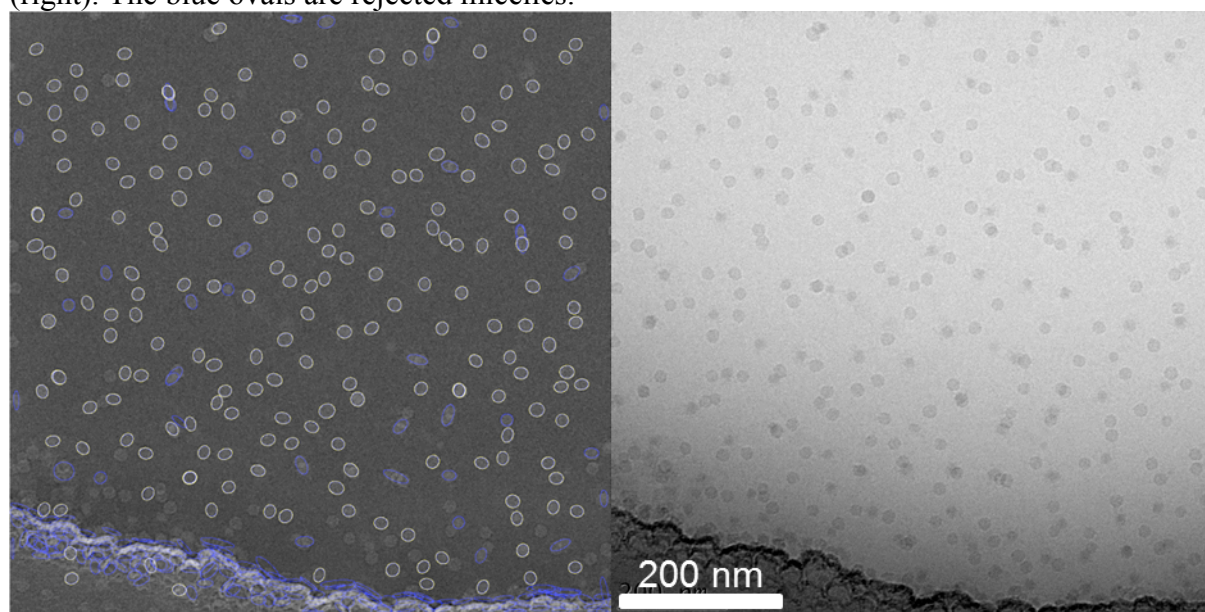


Figure S9. Block-2 micelles as identified by image analysis (left) and as obtained from TEM (right).

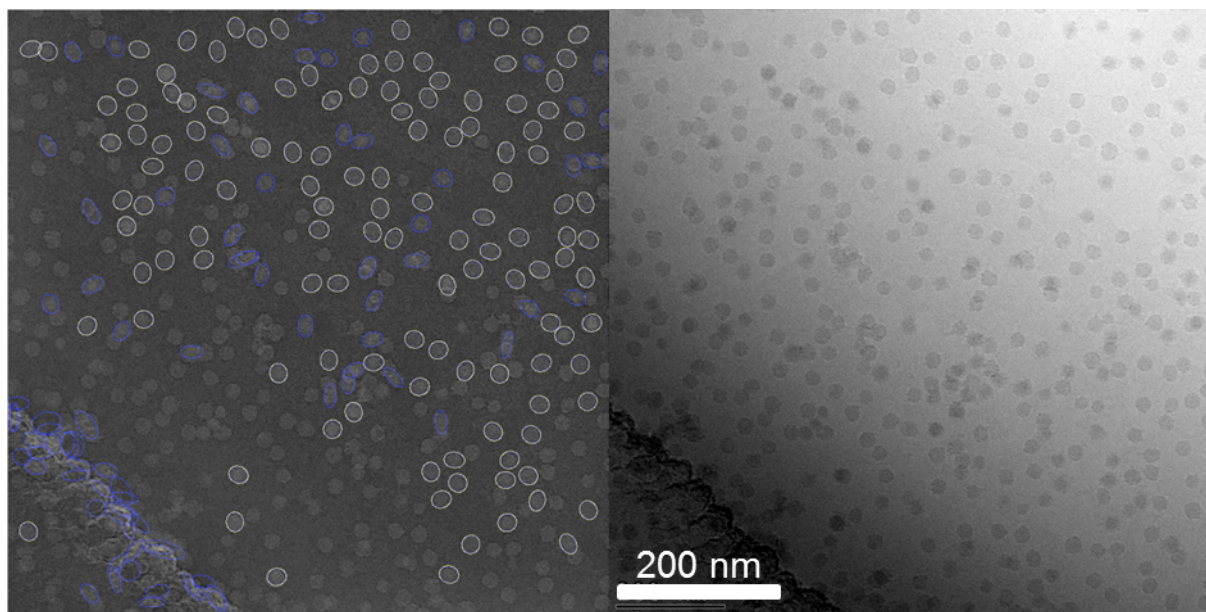


Figure S10. Block-3 micelles as identified by image analysis (left) and as obtained from TEM (right).

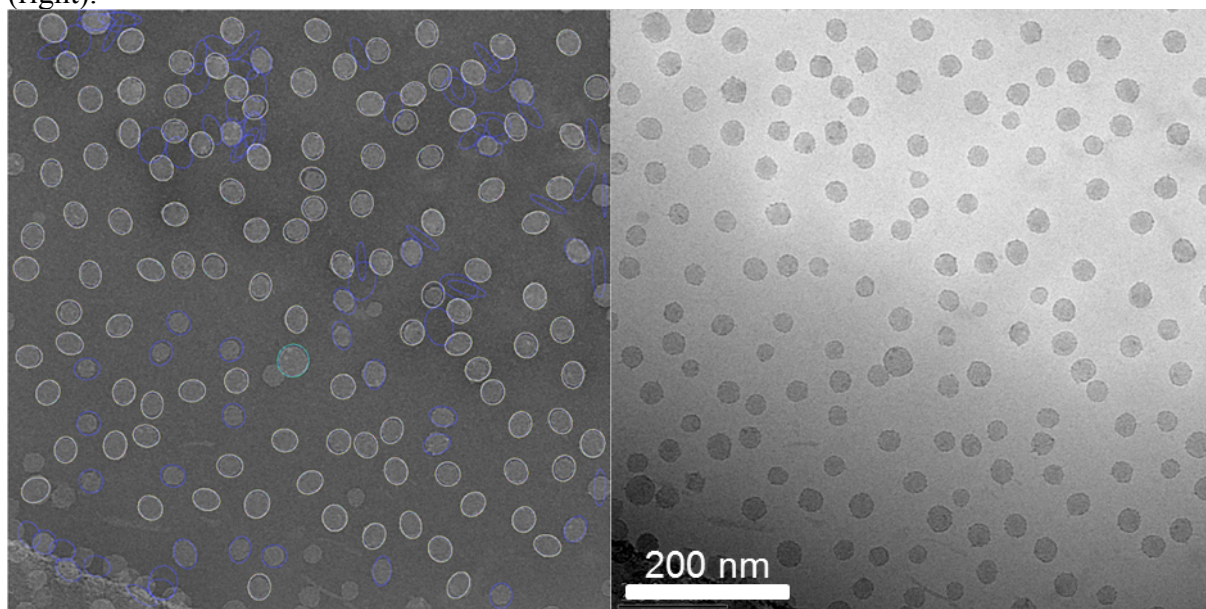


Figure S11. Block-4 micelles as identified by image analysis (left) and as obtained from TEM (right).

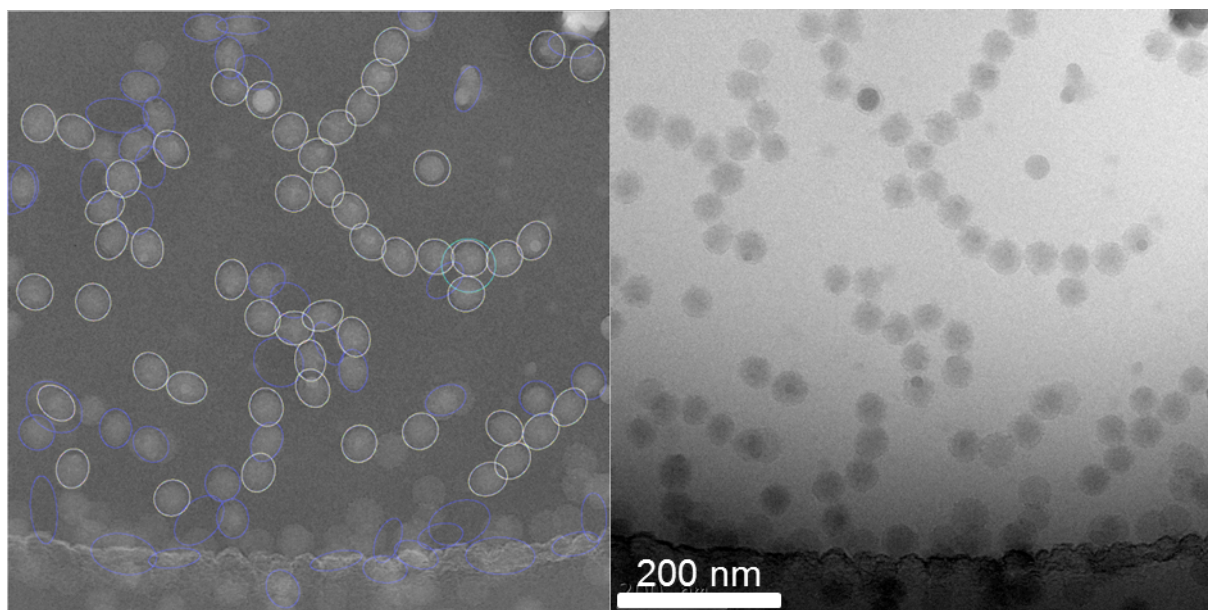


Figure S12. Block-5 micelles as identified by image analysis (left) and as obtained from TEM (right).

Table S2. The diameters of the micelle particles analyzed from TEM images. The diameter as identified by image analysis (*Diameter*), standard deviation of the image analysis (\pm) and number of analyzed micelles (*N*).

	Diameter [nm]	\pm [a] [nm]	N[b]
Block-1	8.4	0.2	1858
Block-2	14.8	0.2	1070
Block-3	21.3	0.1	892
Block-4	28.4	0.2	429
Block-5	41.8	0.6	173

[a] standard deviation [b] number of analyzed micelles

S7. Dynamic light scattering data

Table S3. The diameters of the micelles were analyzed by DLS. The determination was made both with and without 1 mM NaHCO₃ buffer. Instrument gave two distinct values: most probable size for the particle (*peak*) as well as the commonly reported Z-average size (*Z-ave*). Error <10%.

	10 ⁻⁵ M ionic strength		10 ⁻³ M ionic strength	
	Peak[a] [nm]	Z-ave[b] [nm]	Peak[a] [nm]	Z-ave[b] [nm]
Block-1	12	10	12	11
Block-2	22	18	18	15
Block-3	24	16	15	13
Block-4	73	97	81	67
Block-5	38	30	61	57

[a] The most probable Gaussian fit for the micelle. [b] Z-average results.

S8. Contact angles

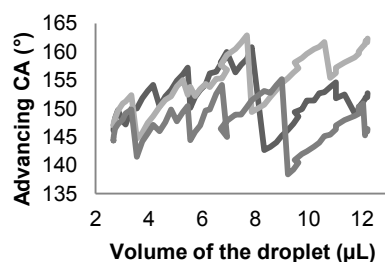


Figure S13. The advancing contact angles (CA) of Block-2 paper (heat treated). The contact angle varies between 140-160°. The peak values 150-160° correspond to the advancing contact angle.

Table S4. Contact angles of the paper samples. The advancing (*Adv. CA*), initial (*In. CA*) and final (*Fin. CA*) contact angles of the heat treated paper samples as well as the advancing contact angles of the room temperature dried paper samples with non-zero contact angles. The receding angles (*Rec. CA*) could not be measured with sufficient accuracy, but were less than 20°.

	Adv.CA [°]	± [°]	In. CA [a] [°]	± [°]	Fin.CA [b] [°]	± [°]	Rec.CA [°]
Ref.	—	—	21	5	0	0	<20
Block-1	—	—	48	12	0	0	<20
Block-2	151	5	102	9	101	11	<20
Block-3	148	10	120	14	109	2	<20
Block-4	148	5	111	2	111	1	<20
Block-5	145	5	112	4	105	4	<20
Block-4 RT	121	9	—	—	—	—	<20
Block-5 RT	123	6	—	—	—	—	<20

[a] Sessile Drop method: Initial contact angles [b] Final contact angles (after 20 sec)

Table S5. Contact angles of the mica samples. The advancing (*Adv. CA*), static (*Sta. CA*) and receding (*Rec. CA*) contact angles of the room temperature dried and heat treated mica samples. Some receding angles (*Rec. CA*) could not be measured with sufficient accuracy, but were less than 10°.

	Adv. CA [a] [°]	± [°]	Sta. CA [b] [°]	± [°]	Rec. CA [c] [°]	± [°]
Ref.	—	—	5	1	<10	
Ref. RT	—	—	12	1	<10	
Block-1 RT	54	2	39	3	<10	
Block-2 RT	47	2	29	4	<10	
Block-3 RT	49	4	30	5	<10	
Block-4 RT	46	6	31	5	<10	
Block-5 RT	39	1	29	5	<10	
Ref. 130 °C	—	—	21	1	<10	
Block-1 130 °C	50	2	45	3	21	4
Block-2 130 °C	79	2	61	4	27	1
Block-3 130 °C	93	1	71	6	22	4
Block-4 130 °C	85	1	68	6	36	1
Block-5 130 °C	85	2	72	4	27	1

[a] Advancing contact angles [b] Static contact [c] Receding contact angle

REFERENCES

- [S1] L. Wågberg, L. Ödberg, G. Glad-Nordmark, L. Odberg, *Nord. Pulp Pap. Res. J.* **1989**, 4, 71.
- [S2] Z. Gao, S. K. Varshney, S. Wong, A. Eisenberg, *Macromolecules* **1994**, 27, 7923–7927.
- [S3] K. Ovaska, M. Laakso, S. Haapa-Paananen, R. Louhimo, P. Chen, V. Aittomäki, E. Valo, J. Núñez-Fontarnau, V. Rantanen, S. Karinen, K. Nousiainen, A.-M. Lahesmaa-Korpinen, M. Miettinen, L. Saarinen, P. Kohonen, J. Wu, J. Westermarck, S. Hautaniemi, *Genome Med.* **2010**, 2, 65.
- [S4] T. Lindeberg, *Int. J. Comput. Vis.* **1998**, 30, 77–116.